Enhanced rockwall retreat and modified rockfall magnitudes/frequencies in deglaciating cirques from a 6-year LiDAR monitoring.

Ingo Hartmeyer[1], Markus Keuschnig[1], Robert Delleske[1], Michael Krautblatter[2], Andreas Lang[3], Lothar Schrott[4], Jan-Christoph Otto[3]

[1]GEORESEARCH Research Institute, Wals, 5071, Austria
[2]Chair of Landslide Research, Technical University of Munich, Munich, 80333, Germany
[3]Department of Geography and Geology, University of Salzburg, Salzburg, 5020, Austria
[4]Department of Geography, University of Bonn, Bonn, 53115, Germany

Correspondence to: Ingo Hartmeyer (ingo.hartmeyer@georesearch.ac.at)

Abstract. Cirque erosion contributes significantly to mountain denudation and is a key element of glaciated mountain topography. Despite long-standing efforts, rates of rockwall retreat and the proportional contributions of low-, mid- and high magnitude rockfalls have remained poorly constrained. Here, a unique, terrestrial LiDAR-derived rockfall inventory (2011-2017) of two glaciated cirques in the Hohe Tauern Range, Central European Alps, Austria is analysed. The mean cirque wall retreat rate of 1.9 mm a^{-1} ranks in the top range of reported values and is mainly driven by enhanced rockfall from the lowermost, freshly deglaciated rockwall sections. Retreat rates are significantly elevated over decades subsequent to glacier downwasting. Elongated cirque morphology and recorded cirque wall retreat rates indicate headward erosion is clearly outpacing lateral erosion, most likely due to the cataclinal backwalls, which are prone to large dip-slope failures. The rockfall magnitude-frequency distribution – the first such distribution derived for deglaciating cirques – follows a distinct negative power law over four orders of magnitude. Magnitude-frequency distributions in glacier-proximal and glacier-distal rockwall sections differ significantly due to an increased occurrence of large rockfalls in recently deglaciated areas. In this paper we show how recent climate warming shapes glacial landforms, controls spatiotemporal rockfall variation in glacial environments and indicates a transient signal with decadal scale exhaustion of rockfall activity immediately following deglaciation crucial for future hazard assessments.

1 Introduction

Cirque erosion contributes significantly to the morphological appearance of glaciated mountain ranges. It controls rockwall retreat and creates emblematic high-alpine landform features such as horn-type peaks and sharp-edged ridges. Erosional processes operating in glacial cirques are widely recognized as important agents of high-alpine landscape evolution (Benn and Evans, 2010; Sanders et al., 2012; Scherler, 2014). Rockfall from cirque walls represents a primary source of debris for glacial systems and thus supplies tools for effective glacial erosion (Hallet, 1981). The disposal of sediment from cirque walls also

represents a prominent entry point to the high-alpine sediment cascade and is, therefore, key to understanding of high-alpine sediment flux (Hales and Roering, 2005; Krautblatter et al., 2012).

Cirque wall retreat is governed by rock slope failure, which can be statistically characterized by their magnitude-frequency distribution (Dussauge et al., 2003; Bennett et al., 2012). Magnitude-frequency distributions are widely used to derive

35 probabilistic recurrence rates of an event of a given size (Dussauge-Peisser et al., 2002) and are key to understanding process efficiency. Mass movement size-distributions can usually be described by a power law (Hovius et al., 1997). Magnitude-frequency distributions of rockfall reflect rock mass properties and triggering mechanisms, and therefore change over time (Krautblatter and Moore, 2014). They constitute an important tool for understanding headwall geomorphology (Densmore et al., 1997), slope response to climatic and environmental change (Schloegel et al., 2011), sediment transport rates (Korup, 2005)

40 and hazard potential (Krautblatter and Moser, 2009). Elevated rockfall activity from freshly excavated rockwalls, such as investigated here, is of major concern in all high-mountain regions, particularly where human pressure increases (Fischer et al., 2011; Purdie, 2013). Due to continuing climate warming its importance is expected to increase throughout the foreseeable future, making accurate knowledge of magnitude-frequency distributions essential for effective risk assessment throughout mountain regions and safeguarding high-alpine infrastructure (Arenson et al., 2009; Bommer et al., 2010).

45 High-alpine cirques were first studied in the early 20th century when cirque walls were considered to wear back through sapping at the base of the headwall and inside the Randkluft (gap between glacier and headwall) through intense frost weathering (Richter, 1900; Martone, 1901; Johnson, 1904). Subsequently, determining ground thermal conditions at the headwall base underlined the importance of periglacial weathering for cirque wall retreat (Gardner, 1987; Sanders et al., 2012). Additional process like rotational ice-flow (Lewis, 1949; Waldrop, 1964), enhanced quarrying due to subglacial meltwater

50 drainage (Hooke, 1991; Iverson, 1991), strong abrasion under thick ice (Strøm, 1945), and slope collapse (Evans, 1997) are also considered key agents of cirque expansion. Numerous allometric studies have focused on cirque morphometry and found remarkably similar cirque length and width across a number of mountain ranges (see review in Barr and Spagnolo, 2015). Deviations from the typical circular cirque-planform were mainly encountered where isometric cirque growth is modified by bedrock lithology (Bennett and Glasser, 2009; Evans, 2006). Despite an extensive research focussing on cirques, cirque erosion

55 is still poorly constrained and the number of published erosion rates has remained limited (e.g. Larsen and Mangerud, 1981; Brook et al., 2006; Sanders et al., 2013).

Inventories of rockfall and rock slope failures in high-alpine environments cover a wide range of spatial and temporal scales. Studies typically focus on catchment scale (Cossart et al., 2008; Krautblatter et al., 2012) or orogen scale (Noetzli et al., 2003; Allen et al., 2011) and mid- to high-magnitude events. Methods used to compile inventories are divers and include field

60 mapping and aerial photograph interpretation (Holm et al., 2004; Fischer et al., 2012), information from observer networks (Ravanel et al., 2010), comparisons of historical and recent photographs (Ravanel and Deline, 2010) and direct observations (Fischer et al., 2006).

Comprehensive quantitative studies that also consider low-magnitude events and thus comprise the entire rockfall spectrum are rare. First approaches date back to the middle 20th century (Rapp, 1960). Over the last two decades, the emergence of

65   LiDAR led to a marked increase of quantitative, high-resolution rockfall studies (Derron and Jaboyedoff, 2010) and provided new insights on rockfall magnitude-frequency distributions (Abellán et al., 2011). However, due to limited resolution LiDAR systematically undersamples the smallest magnitudes (rockfall particles < 10 cm) (Lim et al., 2010), which in some geological settings contribute significantly to rock slope mass wasting (Krautblatter et al., 2012).

Detailed multiannual LiDAR inventories to investigate magnitude-frequency distributions of rockfall were compiled for
70   coastal cliffs (Rosser et al., 2005; Lim et al., 2006), volcanic rock slopes (Nguyen et al., 2011), granitic and limestone rockwalls (Stock et al., 2011; Strunden et al., 2015), and in urban areas (Abellán et al., 2011). Such studies have focussed on precursory events and pre-failure deformation (Rosser et al., 2007; Abellán et al., 2010), disintegration monitoring of single rock slope failures (Oppikofer et al., 2008; Oppikofer et al., 2009), evaluation of rock masses near infrastructure (Hungr et al., 1999; Lato et al., 2012) and analysis of long-term rockwall retreat (Heckmann et al., 2012; Strunden et al., 2015).

75   For glaciated cirques, no rockfall magnitude-frequency distributions have been reported so far. Other steep bedrock environments that have been targeted are coastal cliffs (Williams et al., 2018), small river basins (Bennett et al., 2012), gorge systems (Dussauge-Peisser et al., 2002) and valley flanks (Guzzetti et al., 2003). Rockfall studies in cirque environments either focused on large singular events (Rabatel et al., 2008), on rockfall around infrastructures (Ravanel et al., 2013), or on spatially limited sections of (deglaciating) cirques (Kenner et al., 2011). Spatiotemporal rockfall patterns and rockwall retreat rates for
80   entire cirques over several years have not yet been reported. Despite research efforts reaching back more than 100 years, contemporary cirque wall retreat rates and the efficiency of specific magnitudes have remained unconstrained representing a significant problem for landscape evolution studies and a challenge for rockfall risk management (Brocklehurst and Whipple, 2002; Benn and Evans, 2010; Scherler, 2014).

Here we address this research gap by analysing data from a comprehensive, high-alpine terrestrial LiDAR monitoring
85   campaign (2011-2017), carried out in the rockwalls of two neighbouring, glacierized cirques in the Hohe Tauern Range, Central Alps, Austria (Hartmeyer et al., submitted). We (i) identify significantly increased cirque wall dismantling in the vicinity of the current glacier surface, (ii) observe mean cirque wall retreat rates that rank among the highest values reported yet, (iii) reveal that headward erosion outpaces lateral erosion consistent with present cirque shape, (iv) quantify the first ever magnitude-frequency distribution from a deglaciating cirque, and (v) demonstrate how a wave of instability follows current
90   glacier downwasting. Results are framed in the existing knowledge on magnitude-frequency relationships and considering effects of continuing climatic changes.

2 Study Area

Two neighbouring glacial cirques at the Kitzsteinhorn, Central European Alps, Austria (Fig. 1) were chosen as study site. The two north-facing cirques (~ 0.3 km²), referred to as eastern cirque and western cirque, constitute the root zone of the
95   Schmiedingerkees glacier (~ 0.8 km²), which has retreated considerably in recent years. Currently, the receding ice masses are constraint within the cirques, a state that is characteristic for many glaciers in the Eastern European Alps (Fischer et al., 2018).

Adjacent to the investigated rockwalls, warming-related glacial thinning has led to downwasting rates around 0.5 m per year over the last decade leading to the exposure of fresh cirque wall sections (Hartmeyer et al., submitted). Mean annual air temperature and annual precipitation, both measured at a local weather station situated on the upper part of the

100 Schmiedingerkees glacier (2,940 m a.s.l.), vary around -2 °C and 2,500 mm, respectively. Local borehole temperature monitoring demonstrates the existence of permafrost with temperatures of -1.8 °C (north-facing) and -1.3 °C (west-facing) at zero annual amplitude depth.
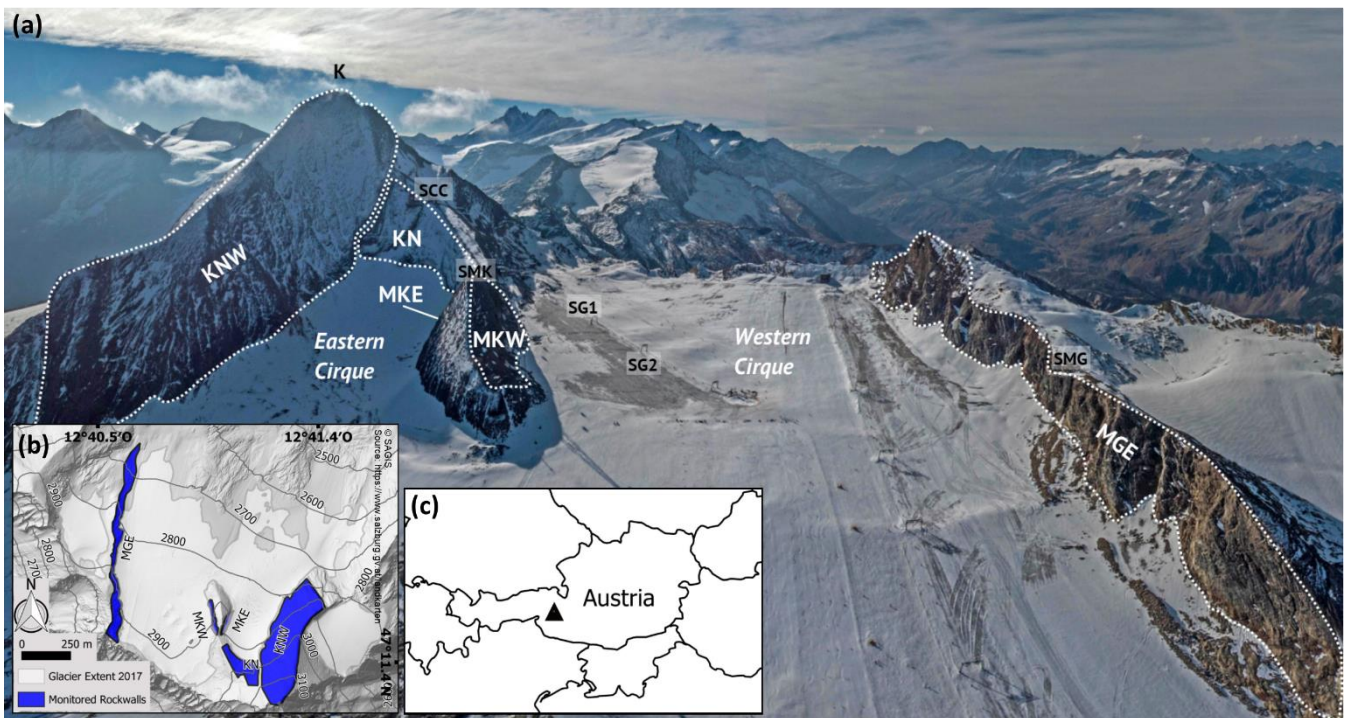
Figure 1: UAV view of rockwalls investigated (surface area, elevation above sea level, mean gradient are indicated in brackets): KN
105 **(23,500 m²; 2,920-3,060 m a.s.l.; 47°), KNW (133,400 m²; 2,770-3,200 m a.s.l., 44°), MKE (11,100 m²; 2,850-2,950 m a.s.l., 71°), MKW (6,300 m²; 2,880-2,940 m a.s.l.; 63°), MGE (60,400 m²; 2,740-2,990 m a.s.l.; 61°) (Photo: Robert Delleske). 1b: Hillshade of study area with monitored rockwalls (blue) and glacier extent. 1c: Location of study area within Austria. Abbreviations: K = Kitzsteinhorn (Summit), SMK = Scan Position 'Magnetkoepfl', SCC = Scan Position 'Cable Car Top Station', SG1 = Scan Position 'Glacier 1', SG2 = Scan Position 'Glacier 2', SMG = Scan Position 'Maurergrat', see text for further abbreviations (Photo: UAV/R. Delleske).**

110 The Schmiedingerkees glacier and the immediately adjacent summit pyramid of the Kitzsteinhorn constitute one of Austria's most frequented high-alpine tourist destinations with close to one million visitors per year. The Kitzsteinhorn hosts an extensive research site to investigate the consequences of climate change on high-alpine infrastructure and rock stability ('Open-Air-Lab Kitzsteinhorn'). Measurements performed at the Kitzsteinhorn focus on rockfall activity (Keuschnig et al., 2015), subsurface temperature changes (Hartmeyer et al., 2012), geophysical monitoring with ERT (Supper et al., 2014;

115 Keuschnig et al., 2016), rock mass pressure using anchor load plates (Plaesken et al., 2017) and fracture dynamics monitoring with crackmeters (Ewald et al., 2019).

Full details of the study site are presented in Hartmeyer et al., submitted. In brief, the total surface area of the investigated rockwalls is 234,700 m² and their mean vertical extent ranges between 35-200 m. All studied cirque walls are immediately adjacent to the Schmiedingerkees glacier: In the eastern cirque the Kitzsteinhorn north-face (KN) (backwall), Kitzsteinhorn

120 northwest-face (KNW) and Magnetkoepfl east-face (MKE) (sidewalls). In the western cirque no significant backwall exists and the Magnetkoepfl west-face (MKW) and Maurergrat east-face (MGE) were monitored (Fig. 1).

All cirque walls developed in rocks of the Bündner schist formation within the Glockner Nappe and belong to the Glockner Facies consisting of calcareous micaschist, prasinite, amphibolite, phyllite, marble and serpentinite (Cornelius and Clar, 1935; Hoeck et al., 1994). Within the monitored rockwalls, NNE-dipping (~ 45 °) calcareous micaschists dominate, and isolated

125 marble and serpentinite belts exist at Magnetkoepfl. Two distinct joint sets (J1 dipping steep to W, J2 medium-steep to SW) oriented approximately orthogonal to the cleavage precondition disintegration into cubic rock fragments (Fig. 2). Numerous open fractures infilled with fine-grained material enable water infiltration and affect near-surface rock slope kinematics and thermal dynamics (Keuschnig et al., 2016; Ewald et al., 2019). Rock at the surface is highly fractured due to a pronounced frost weathering susceptibility. Strong tectonic forcing resulted in highly fractured weakness zones along major faults in all

130 rockwalls. Rock mass classifications according to Romana, 1985 and Bieniawski, 1993 suggest highly variable lithological strength ranging from low stability values in weakened zones (r = 34) and highly stable conditions in steep, unweathered sections (r = 98) (Terweh, 2012).
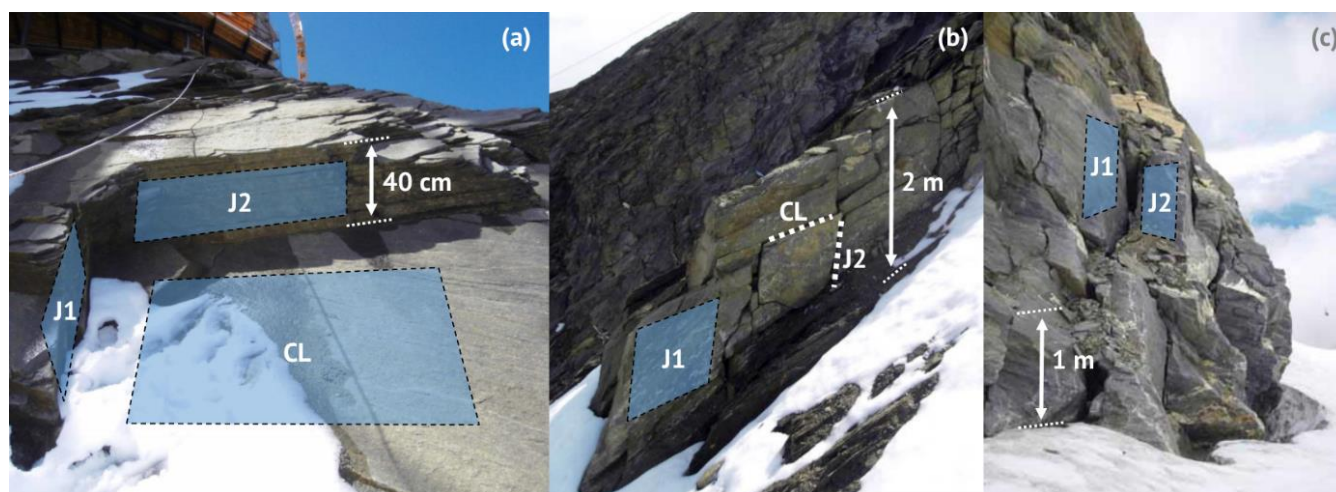
Figure 2: Dominant discontinuity orientations at (a & b) Kitzsteinhorn north face (KN) and (c) at Magnetkoepfl east face (MKE).
135 **Cleavage (CL) of predominant calcareous mica-schists dips about 45° NNE. Joint sets J1 (dipping subvertical to W) and J2 (dipping steeply to SW) are approximately orthogonal to CL and predispose north-facing slopes for dip-slope failures (a, b), while west- and east-facing areas are more susceptible to toppling failures (c) (Photos: Andreas Schober).**

3 Methods

3.1 LiDAR Data Acquisition and Processing

140 Full details of data acquisition can be found in Hartmeyer et al., submitted. In brief, terrestrial LiDAR acquisition was based on a Riegl LMS-Z620i laserscanner equipped with a calibrated high-resolution digital camera to take referenced colour images. Rockwalls were scanned in reflectorless mode at least once a year between 2011 and 2017 at the end of the ablation period. A total of 56 rockwall scans were carried out with variable mean object distances (140-650 m) depending on the used scan position. Resulting point cloud resolution typically ranges between 0.1-0.3 m (see supplement of Hartmeyer et al., submitted

145 (Table S2) for a full list of data acquisition parameters).

Iterative-Closest-Point (ICP) procedures (Chen and Medioni, 1992) were applied for point cloud alignment. Areas that have been subject to surface change between surveys were discarded during the process and therefore do not negatively affect the quality of surface matching (Abellán et al., 2010; Abellán et al., 2011), resulting in alignment errors between 1-2 cm. Surface change between point clouds were identified using the M3C2 algorithm of Lague et al., 2013 due to is robust performance on

150 irregular surfaces, with missing data and changes in point density. Rockfall volumes were estimated for each individual rockfall source area as well as morphometric parameters like slope aspect, gradient and elevation above glacier surface.

3.2 Rockfall Magnitude-Frequency Calculation

Numerous studies (e.g. Hungr et al., 1999) demonstrated that the relationship between rockfall volume and cumulative rockfall frequency can be defined by a power law following Eq. (1):

155 $$f(V) = \alpha V^{-b} \qquad (1)$$

where $f(V)$ is the cumulative number of rockfalls, V is the rockfall volume, and α and b are constants. To test the power-law-fit of an empirical distribution, earlier studies mainly relied on two regression approaches: cumulative distribution functions (CDF) and probability density functions (PDF) (Bennett et al., 2012; Strunden et al., 2015). According to (Bennett et al., 2012) the PDF is better suited to visualize rollovers, i.e. a decrease in the frequency density for small events. It requires, however,

160 logarithmic binning of rockfall volumes that is rather subjective and has been demonstrated to introduce bias in the calculation of power law exponents (Clauset et al., 2009; Bennett et al., 2009). As will be shown in Sect. 4.4, the magnitude-frequency data used here does not show a rollover at low event sizes and so CDFs were constructed using the R package poweRlaw (Gillespie, 2015).

4 Results

4.1 Rockfall Magnitudes

Over the course of the monitoring program, scan positions and acquisition resolution had to be altered resulting in differing data resolution between scans. To enable direct comparison of scans of differing resolution the impact of scan resolution on the number of events detected was constrained. Using a regression analysis it is shown that for events larger than 0.1 m³ scan resolution has no statistically significant impact (Hartmeyer et al., submitted).

Above this threshold, 374 rockfalls were identified resulting in a total volume of 2,551.4 ± 85.3 m³. To classify rockfall volumes, the recorded rockfalls were grouped into bins of logarithmically increasing size to balance against strongly uneven event volumes (Fig. 3). A dominance of large events is evident as two thirds (67 %) of the rockfall volume fall into the largest size class (100-1,000 m³), while the next smaller class (10-100 m³) accounts for approximately one fourth (23 %), and the two smallest classes (0.1-10 m³) combined constitute only about one tenth (10 %) of the total rockfall volume.
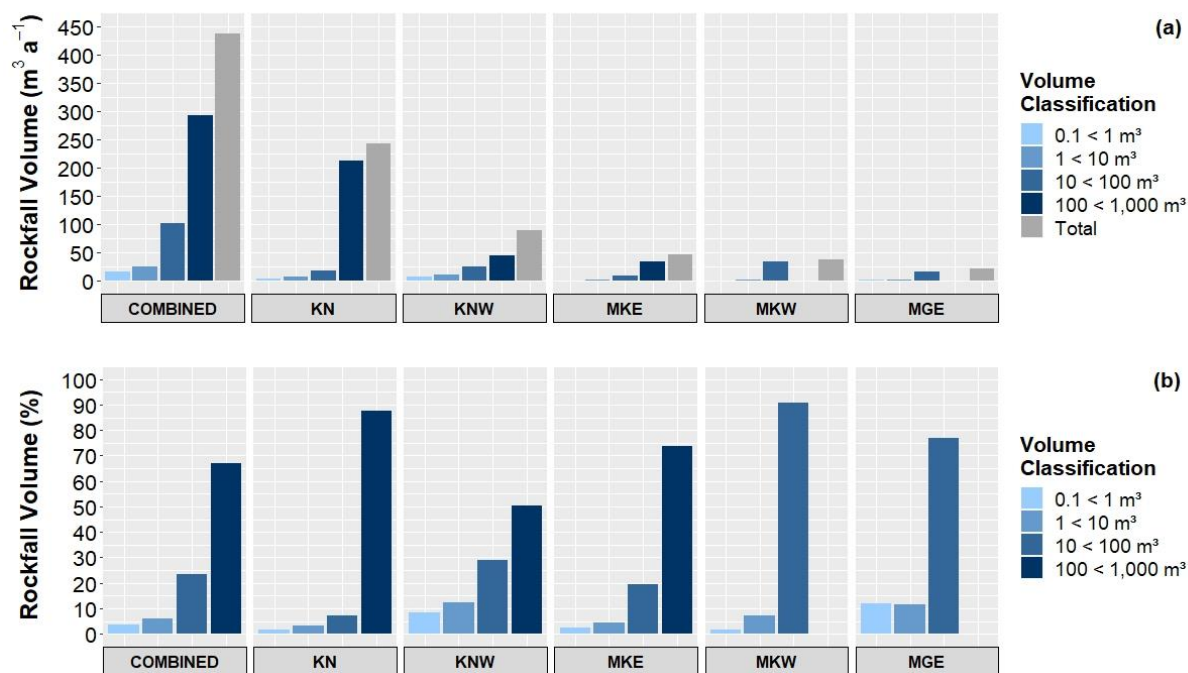
Figure 3: (a) Absolute rockfall volume (m³ a⁻¹), (b) relative rockfall volume (%) for all monitored rockwalls. About two thirds (67 %) of the total rockfall volume fall into the largest size class (100-1,000 m³) reflecting the dominance of large events.

When analysed individually for each rockwall the size distribution shows significant differences due to the impact of individual large rockfalls: At all walls most of the rockfall volume is represented by the largest size classes (at KN rockfalls > 100 m³ contribute 88 %, at MKE and KNW contributions equal 74 % and 50 %, respectively and no rockfalls > 100 m³ occurred at MKW and MGE). The combined share of the two largest size classes (i.e. rockfalls > 10 m³) ranges between 77 % (MGE) and

95 % (KN), whereas the smallest size class (0.1 – 1 m³) represents only around 2 % of the total volume at KN and at the Magnetkoepfl (MKE, MKW) and about 10 % at MGE and KNW.

In a companion study, we demonstrated significantly increased rockfall in the immediate surroundings of the glacier resulting from antecedent rockfall preparation inside the Randkluft and recent glacial downwasting adjacent to the investigated cirque walls (Hartmeyer et al., submitted). This is also evident if the volume classification is further differentiated according to distance from glacier (Fig. 4): At 0-10 vertical meters above the glacier surface ("proximal areas"), rockfalls larger than 100 m³ constitute 84 % of the total volume whereas in rockwall sections located > 10 m above the glacier surface ("distal areas") the contribution of this class drops to just 41 %. Small rockfalls below 1 m³ on the other hand contribute around 1 % to the total rockfall volume in proximal areas, while in distal areas this part increases to 7 %.
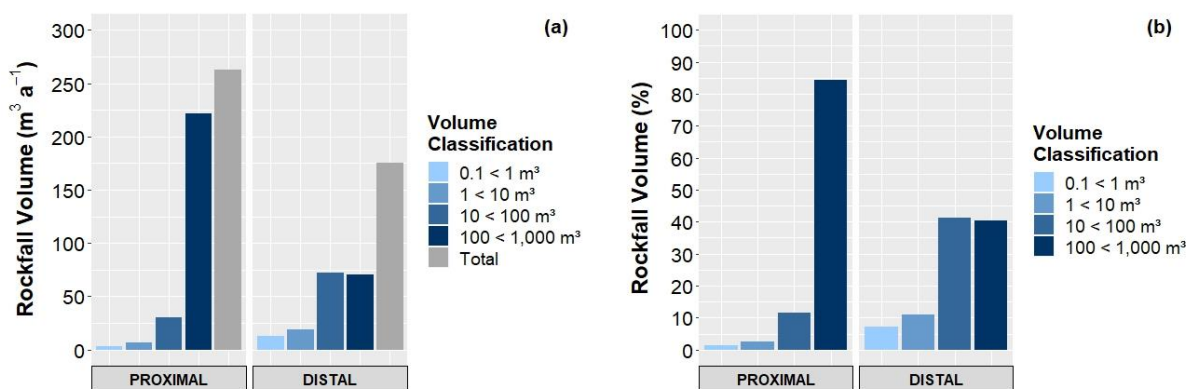
Figure 4: (a) Absolute rockfall volume (m³ a⁻¹), (b) relative rockfall volume (%) for rockwall sections 0-10 vertical meters above the glacier surface ('Proximal') and for higher (> 10 m) rockwall sections ('Distal'). Large events (100-1,000 m³) dominate rockfall size distributions in proximal areas while distal areas show a more balanced distribution.

4.2 Rockwall Retreat Rates

Across the full period of observation and across all rockwalls the mean retreat rate is 1.9 mm a⁻¹. In detail, annual rockwall retreat varies considerably between the rockwalls investigated and is highest along highly fractured weakness zones close to the glacier surface (Hartmeyer et al., submitted). The maximum rate is found at KN (10.4 mm a⁻¹), followed by the two rockwalls of the Magnetkoepfl. At MKW retreat rates equal 5.9 mm a⁻¹, and at MKE 4.2 mm a⁻¹was recorded. Lowest rates were calculated for KNW (0.7 mm a⁻¹) and MGE (0.3 mm a⁻¹) (Fig. 5).

In proximal areas, mean retreat rates of 7.6 mm a⁻¹ are found and in distal areas rates are almost an order of magnitude lower (0.9 mm a⁻¹). By far the highest retreat rates in proximal areas were registered at KN (57.3 mm a⁻¹), followed by MKE (17.0 mm a⁻¹). At KN several large rockfalls were recorded adjacent to the glacier surface along a prominent joint intersection. Following the cleavage direction at MKE a ledge of highly fractured micaschists runs diagonally through the rockwall. Here, the highest instability occurs especially in the immediate vicinity of the glacier surface from where a major share of the rockfall volume originates.

Earth **Surface**
Dynamics
Discussions
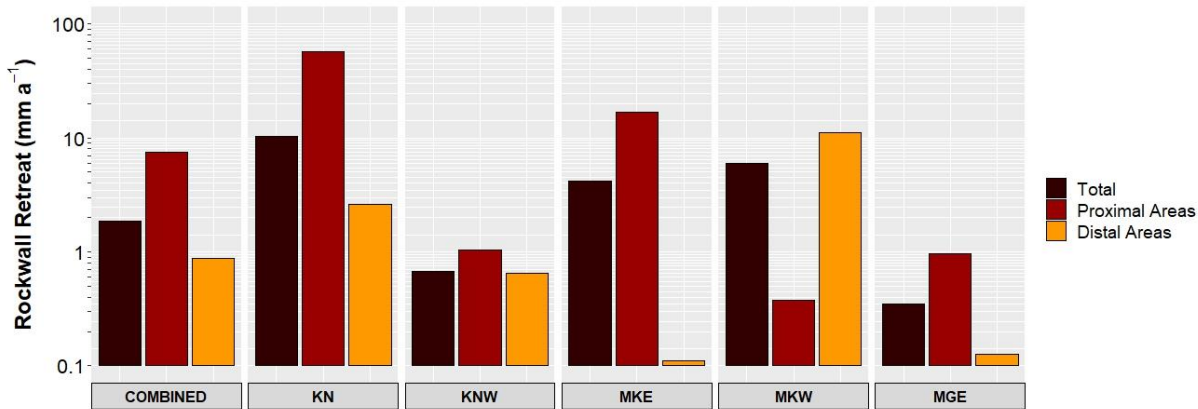
Figure 5: Rockwall retreat rates (mm a⁻¹) (i) for the entire rockwall (dark red), (ii) for proximal areas (0-10 m, red) and (iii) for distal areas (> 10 m, orange). The mean rate over the six-year observation period is just under 2 mm a⁻¹ were found. Rockwall retreat rates in proximal areas (7.6 mm a⁻¹) were almost an order of magnitude higher than in distal areas (0.9 mm a⁻¹).

The highest distal retreat rates are found at MKW (11.1 mm a⁻¹). This is also the only site where retreat rates in the first 10 m are exceeded by retreat rates in more distal sections. due to continuing mass wasting from a rockfall scarp initiated in the 2000s and located about 15 m above the current glacier surface.

4.3 Rockfall Frequencies

To compare rockfall frequency across rockwalls, rockfall numbers were normalized for rockwall size (Fig. 6). Averaged over all five monitored rockwalls, 2.7 rockfalls per 10,000 m² a⁻¹ were registered. Maximum numbers were recorded at KN (n = 7.4) followed by MKW (n = 6.0) while the lowest numbers were found at MGE (n = 1.5).
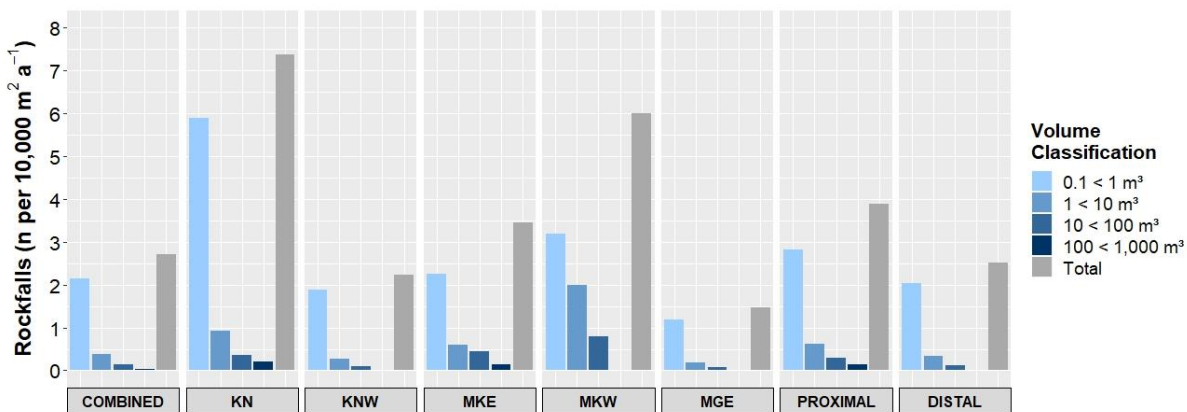
Figure 6: Normalized rockfall numbers (n per 10,000 m² a⁻¹) for all monitored rockwalls. Rockfall frequency decreases exponentially with increasing rockfall size, 80 % of all rockfalls rank in the smallest size class (0.1-1 m³).

Rockfall frequency decreases exponentially with increasing rockfall size. Almost 80 % of all rockfalls fall in the smallest size class (0.1-1 m³) while the next larger size class (1-10 m³) comprises 14 % and the two largest size classes (10-100 m³, 100-1,000 m³) 6 % and 1 %, respectively. The frequency pattern is rather similar for all rockwalls, and only the Magnetkoepfl

rockwalls (MKE, MKW) show some minor deviations. Here, the smallest size class represents a relatively low share (65 %
225 and 53 %, respectively), whereas the larger size classes account for a comparatively high proportion (see supplement of
Hartmeyer et al., submitted (Table S3) for full details).

The difference between rockfall frequency in proximal areas (n = 3.9) and distal areas (n = 2.5) is considerable yet less
pronounced than the (eightfold) difference between proximal (7.6 mm a^{-1}) and distal (0.9 mm a^{-1}) rockwall retreat rates.
Proximal rockfall frequency exceeds distal rockfall frequency for all size classes. The discrepancy between proximal and distal
230 rockfall frequency grows with rockfall size. Rockfalls > 10 m³ constitute 10 % of all proximal rockfalls, where as in distal
areas only around 5 % of all rockfalls exceed 10 m³. Rockfalls > 100 m³ represent around 4 % of all proximal rockfalls (< 1 %
in distal areas) and thus occur 8.6 times more often in proximal areas than in distal areas. Low magnitudes represent a smaller
share in proximal areas (73 %) and a larger share in distal areas (82 %).

4.4 Magnitude-Frequency Distributions
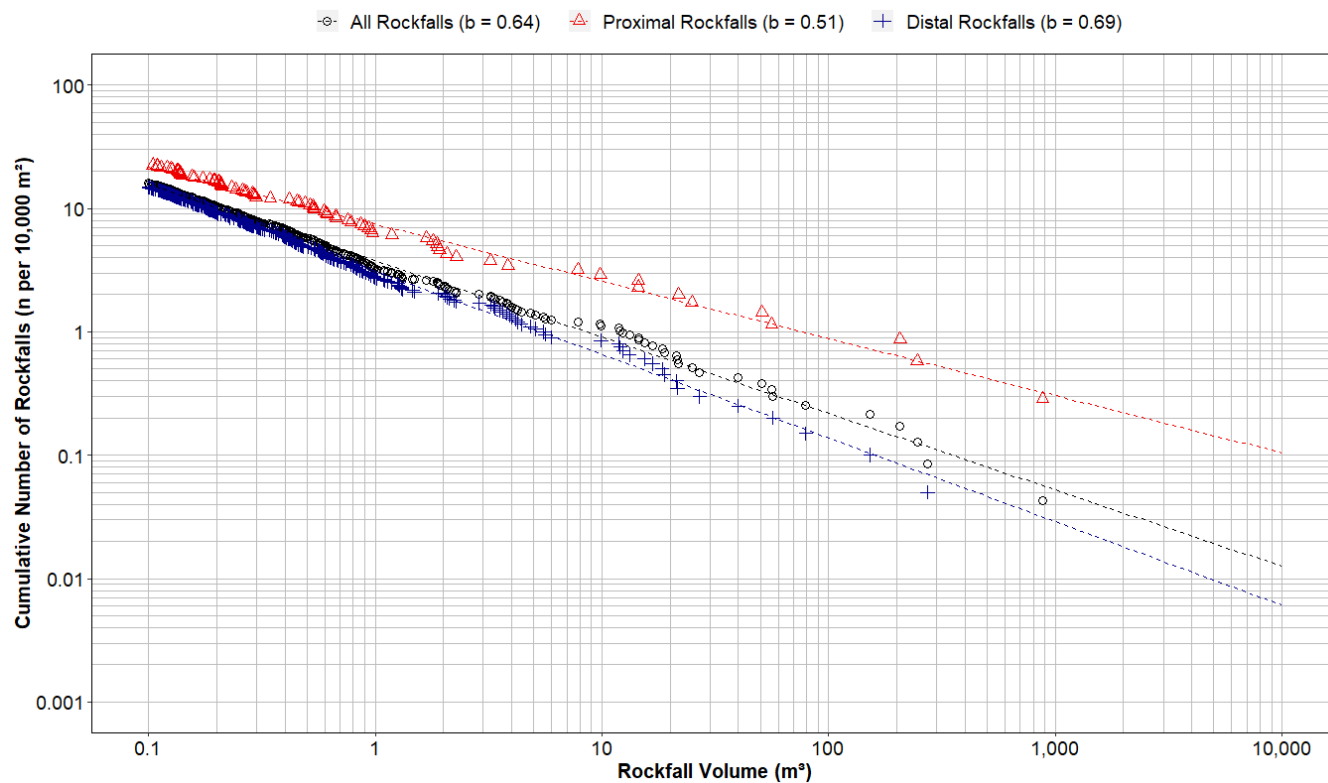
235

Figure 7: Magnitude-frequency distribution for (i) all detected rockfalls, (ii) proximal rockfalls and (iii) distal rockfalls. The power law exponent (b) determines the slope of the regression line (straight line in log-log space). Proximal rockfalls (b = 0.51) are fitted by a flatter regression line than distal rockfalls (b = 0.69) pointing to an increased frequency of large rockfalls in the vicinity of the glacier (i.e. in areas more recently exposed by glacier retreat).

240   To further characterize spatiotemporal rockfall variations, the magnitude-frequency distributions were fitted using a power-law. The resulting distinct negative power law distribution extends over four orders of magnitude and tails off towards high magnitudes. Including all events the power law exponent is b = 0.64 (Fig. 7). Rockfall magnitude-frequency distributions for proximal rockfalls yield an exponent b = 0.51 and for distal rockfalls the exponent b = 0.69. This significant difference between proximal and distal rockfall magnitude-frequency distributions is primarily caused by an increased frequency of large rockfalls

245   in proximal rockwall sections.

5 Discussion

5.1 Cirque Erosion

Erosional processes are both, highly discontinuous and unsteady over time (Sadler, 1981), particularly in paraglacial environments (Ballantyne, 2002; McColl, 2012). Erosion rates recorded during short observation periods are therefore unlikely

250   to accurately reflect long-term rockwall retreat over geological time scales (Krautblatter et al., 2012). High-magnitude events occur with lower frequency and are usually undersampled, contributing to a systematic underestimation of long-term rockwall retreat (e.g. Strunden et al., 2015). Observations made during periods of elevated geomorphic activity result in an overestimation of long-term rates (e.g. Ballantyne and Benn, 1994). Interpretation of short-term erosion records in a broader landscape evolution context thus requires careful consideration of the respective geomorphological setting.

255   To date, only few erosion rate estimates have been reported for cirques (Benn and Evans, 2010; Barr and Spagnolo, 2015). Investigations carried out in cirques in the Sangre de Cristo Range, USA (Grout, 1979), Kråkenes, Norway (Larsen and Mangerud, 1981), the Ben Ohau Range, New Zealand (Brook et al., 2006) and the Rocky Mountains, Canada (Sanders et al., 2013) all report (long-term) erosion rates around or below 1 mm a^{-1}. Recent extensive compilations of rockwall retreat rates from periglacial environments (not restricted to cirques) yield similar results, with rates mostly below 1 mm a^{-1} (de Haas et al.,

260   2015; Ballantyne, 2018).
Direct cross-study comparison is difficult due to differing study designs and key environmental factors (Barr and Spagnolo, 2015). Still, the mean retreat rate at the Kitzsteinhorn of just under 2 mm a^{-1} is one of the highest values published worldwide. Taking it beyond Earth, Kitzsteinhorn results still are at the higher end of a range of time-span corrected terrestrial and extraterrestrial rockwall retreat rates as compiled by de Haas et al., 2015.

265   Higher erosion rates (> 2 mm a^{-1}) were reported for headward cirque erosion in Antarctica (5.8 mm a-1) (Andrews and LeMasurier, 1973), for headwalls above rock glaciers in the Swiss Alps (2.5 mm a^{-1}) (Barsch, 1977), the French Alps (2.5 mm a^{-1}) (Francou, 1988) and West Greenland (5 mm a^{-1}) (Humlum, 2000), for a footwall location at Mt. Eiger in the Swiss Alps (Mair et al., 2019), for a very humid and tectonically active glaciated basin in the Southern Alps of New Zealand (5.6 mm a^{-1}) (Hicks et al., 1990), for selected sections of a deglaciating rocky ridge in the Swiss Alps (6.4 mm a^{-1}) (Kenner et al., 2011) and

270   for cirque-wall sections in the French Alps affected by a single, large rockfall event (8.4 mm a^{-1}) (Rabatel et al., 2008). These results were, however, not derived from cirque-scale monitoring but instead reflect short-term, local erosion rates in selected,

highly active rockwalls. Such data is better compared to the range of maximum headward erosion rates established at the Kitzsteinhorn, the maximum of which is 10.4 mm a^{-1} at KN.

Long-term cirque evolution is considered to show highest erosion rates during the transition to ice-free conditions, when
275   cirques are occupied by small glaciers only. Cirque growth is thus considered being far from a steady process but meant to happen in spurts during deglacial and interglacial periods (Delmas et al., 2009; Crest et al., 2017). The data analysed here and in a companion study (Hartmeyer et al., submitted) confirms such patterns and reveals considerably elevated retreat rates in recently deglaciated glacier-proximal areas (7.6 mm a^{-1}), while more distal rockwall sections show retreat rates of less than 1 mm a^{-1} (Fig. 5). Despite the intrinsically difficult comparison of geomorphic evidence from vastly different spatiotemporal
280   scales, our findings indicate enhanced cirque growth during deglaciation. Two subsequent process-sets potentially underscore the geomorphic significance of deglaciation-related rockfall and the correlation between glacier retreat and cirque wall dismantling. Firstly, initial thermomechanical stresses due to deglaciation-induced rock mass damage condition instabilities that persist far beyond the actual deglaciation (Graemiger et al., 2018); and secondly, the substantial input of fresh rockfall debris to the randkluft and into the sliding glacier base is likely to cause enhanced subglacial erosion and thus drive cirque
285   erosion also over longer time scales (Sanders et al., 2013).

Rockwall retreat primarily advances along major joint intersections (Sass, 2005; Moore et al., 2009; Hartmeyer et al., submitted) and therefore rockfall activity varies considerably spatially across cirque walls (Fig. 5). The highest rates overall were recorded at KN, the only of the five monitored rockwalls where inclination follows cleavage dip (~ 45 °N) and enables significant dip-slope failures of large cubic rock fragments (Fig. 2). High rates were also recorded at the Magnetkoepfl (MKW,
290   MKE) where instability in part results from intense glacial strain during past glaciations due to the Magnetkoepfl's location between two ice flows (Fig. 1) providing intense abrasion.

During the six-year monitoring period headward cirque erosion at KN (10.4 mm a^{-1} overall, 57.3 mm a^{-1} in proximal areas) exceeded lateral cirque erosion at KNW/MKE/MKW/MGE (0.9 mm a^{-1} overall, 2.3 mm a^{-1} in proximal areas) by an order of magnitude. At the western cirque (sidewalls MKW, MGE), only small remnants of a backwall exist, exhibiting a similar,
295   cataclinal discontinuity setup as KN. While this specific area was not monitored in the present study, the absence of a significant backwall provides clear evidence for intense headward erosion in the past predisposed by the mica-schist cleavage. The eastern cirque – confined by backwall KN and sidewalls KNW, MKE – and to a lesser degree the western cirque, display clear north-south elongated shapes (Fig. 1). These morphologies indicate that due to highly effective cleavage-driven sapping the headward cirque erosion (north faces) has outpaced lateral cirque erosion (west and east faces) over extended time periods.
300   The cataclinal backwalls thus not only affect short-term rockfall dynamics but also have a substantial effect on long-term erosion patterns that carved today's elongated cirque (Andrews and LeMasurier, 1973; Oskin and Burbank, 2005), which deviates significantly from ideal circular shapes found in several orogen-scale studies of cirque allometry (Federici and Spagnolo, 2004; Evans, 2006).

5.2 Rockfall Magnitudes and Frequencies

305 Many earlier studies have deduced magnitude-frequency distributions to statistically describe spatiotemporal rockfall variation in various non-glacial environments (Dussauge-Peisser et al., 2002; Malamud et al., 2004). Here we present the first rockfall magnitude-frequency distribution for a deglaciating cirque (Fig. 7) that also shows characteristic negative power functions between rockfall number and rockfall volume (Hovius et al., 1997; Hungr et al., 1999; Stark and Hovius, 2001).

During the monitoring period about two thirds of the rockwall retreat resulted from low-frequency rockfalls > 100 m³, while
310 smaller high-frequency events being of minor relevance only (Fig. 3). At low magnitudes, no rollover (i.e. drop-off in rockfall frequency) was registered. Rollovers are more frequent in landslide inventories (Malamud et al., 2004) but have also been reported for rockfall inventories (Strunden et al., 2015). Their existence has been attributed to physical causes (Bennett et al., 2012), more frequently also as indicative of undersampling small failures due to insufficient spatial resolution (Stark and Hovius, 2001). The absence of a rollover in the inventory presented emphasizes consistent data quality and confirms an
315 unbiased identification of rockfalls down to (at least) the cutoff threshold of 0.1 m³.

The contribution of rockfalls smaller than the specified size threshold of 0.1 m³ remains uncharacterized. Extending the power law established to the unspecified space below the 0.1 m³ cutoff threshold demonstrates that the unexamined small-magnitude rockfalls do not provide a significant contribution to the total mass wasting budget. Rock slope erosion in the two studied cirques is therefore dominated by the upper end of the investigated magnitude spectrum, which provides a valuable contribution
320 to an ongoing debate that dates back to the origins of quantitative research on rockwall retreat (Heim, 1932; Jaeckli, 1957).

To test the robustness of the analyses and the sensitivity of the regression to individual rare events, the power-law-fits were recalculated after omitting the five largest events (rockfalls > 100 m³) from the data set. The results show only minor deviations with slightly increased power law exponents (+0.03) for the magnitude-frequency distribution using the reduced dataset (+0.08 for proximal rockfalls, +0.02 for distal rockfalls). The large rockfalls recorded (100-1,000 m³) do not fundamentally alter the
325 regression underlining the robustness of the magnitude-frequency relationship.

Ignoring lithological and topographic constraints and extrapolating the power law beyond the upper end of the observed magnitude spectrum (~ 1,000 m³) allows rough estimates of recurrence intervals of high-magnitude events. For rockfalls ≥ 10,000 m³ a return period of around 20 years is indicated while rockfalls ≥ 100,000 m³ recur once in a century. With increasing rockfall magnitude proximal and distal regression lines increasingly diverge. Normalized for rockwall size, rockfalls ≥ 10,000
330 m³ are almost 20 times more likely in proximal rockwall sections than in distal rockwall sections (40 times more likely for rockfalls > 100,000 m³) (Fig. 7).

Values of the power law exponent b reported in the literature correlate negatively with lithological strength, as larger events are getting less frequent as slope strength decreases. Smaller exponents are typically observed in stronger bedrock, whereas high values correspond either to slopes of weaker bedrock or to soil-mantled slopes (Bennett et al., 2012). Exponents for
335 landslide inventories (b ~ 1-1.5) are therefore significantly higher than exponents for rockfall inventories, which typically range between 0.1-1 (Dussauge et al., 2003; Bennett et al., 2012). The power law exponent calculated here for distal rockwall

sections (b = 0.69) falls in the upper range observed for rockfall distributions and clearly below the range determined for landslides. The high exponent is caused by (i) the rather high bedrock erodibility of the local calcareous micaschists (Terweh, 2012), and (ii) highly fractured zones with low lithological strength along structural weaknesses that are highly susceptible to

340   rockfall (Hartmeyer et al., submitted; Sass, 2005; Moore et al., 2009).

Beside lithological strength, differences in power law exponents between different studies may also be related to the temporal data resolution (given here by the survey interval). Longer return periods between surveys increase the probability of superimposition and coalescence of events and result in decreasing failure numbers and increasing failure volumes, and thus lower power law exponents (Barlow et al., 2012). Recent near-continuous LiDAR monitoring of cliff erosion highlights how

345   different return periods between surveys affect magnitude-frequency distributions (Williams et al., 2018). While frequent monitoring provides more realistic magnitude-frequency distributions, longer durations between scans increase data precision and are advantageous for quantifying longer-term erosion rates due to reduced accumulative uncertainties (van Veen et al., 2017; Williams et al., 2018).

The significant differences between magnitude-frequency distributions in proximal areas (b = 0.51) and distal areas (b = 0.69)

350   cannot be related to variations in lithology or sampling interval but result from the destabilizing effect of recent ice retreat. Following deglaciation, pronounced thermal stress is induced and an active layer penetrates into the exposed bedrock (Hartmeyer et al., submitted; Draebing and Krautblatter, 2019) contributing to an increased rockfall frequency close to the glacier surface. Variations between rockfall magnitude-frequency distributions in (proximal) areas directly affected by deglaciation and (distal) areas unaffected by recent deglaciation become most apparent at the upper end of the magnitude

355   spectrum investigated: The (normalized) frequency of rockfalls > 100 m³ is almost ten times higher in proximal areas than in distal areas (Fig. 6). The increased occurrence of large rockfalls in the vicinity of the glacier leads to a flatter regression line and thus to a reduced power law exponent for proximal areas. In distal areas large rockfalls are of reduced importance and the rockfall volume distribution here peaks at lower magnitudes, potentially contributing to a pattern that has been described as "archway-shaped" distribution in earlier studies (Krautblatter et al., 2012).

360   The results clearly show how recent climate warming modifies spatiotemporal rockfall occurrence in glacial environments over decades subsequent to glacier downwasting. The patterns obtained are important for rockfall hazard assessments as they indicate that in rockwalls affected by glacier retreat historical rockfall patterns may no longer be used as indicators for future events (Sass and Oberlechner, 2012; Krautblatter and Moore, 2014). Implications for risk assessment are particularly critical in cirque environments, where the presence of glacially oversteepened rockwalls and low-friction glacier surfaces promote

365   long rockfall runout distances (Schober et al., 2012). Many high-alpine, glacier tourism areas that are enjoying growing popularity worldwide, may have to adapt risk-reduction measures in the near future (Purdie et al., 2015).

6 Conclusions

A unique six-year rockfall inventory (2011-2017) from the lateral and back-walls of two elongated glaciated cirques in the Hohe Tauern Range, Central European Alps, Austria provides unique insights into rockfall dynamics in deglaciating terrain. The inventory was derived from detailed terrestrial LiDAR data and represents the most extensive high-resolution compilation of rockfall in cirque walls. Besides significantly increased rockfall occurrence close to the glacier surface due to rockfall preconditioning inside the Randkluft and ice surface lowering (Hartmeyer et al., submitted), the analysis of cirque wall retreat and rockfall magnitude-frequency distributions clearly indicates:

- High mean cirque wall retreat of 1.9 mm a^{-1} ranking in the top of reported values worldwide;
- Rockfall activity is boosted in the freshly exposed rock surfaces above the glacier;
- Pre-existing structural weaknesses modify spatial patterns of rockfall activity;
- For glacier-proximal (0-10 m above glacier surface) areas mean retreat rates are an order of magnitude higher than, for distal areas (> 10 m);
- Enhanced cirque wall dismantling in recently deglaciated rockwall sections supports concepts of increased cirque growth during deglacial periods;
- Elongated cirque morphology fits to the pattern in cirque wall retreat rates indicating that headward erosion (10.4 mm a^{-1} at KN) outpaces lateral erosion
- (0.9 mm a^{-1} combined mean for all sidewalls) significantly. The essential factor is the direction of cleavage so that in cataclinal backwalls large dip-slope failures are facilitated and drive effective headward sapping;
- The rockfall magnitude-frequency distribution in the deglaciating cirque follows a clear negative power law distribution over four orders of magnitude (b = 0.64);
- Rockfall magnitude-frequency distributions in glacier-proximal areas (b = 0.51) and distal areas (b = 0.69) differ significantly and demonstrate a greater importance of large rockfalls in recently deglaciated rockwalls;
- Climate warming enhances rockfall occurrence in glacial environments; a persistent pattern that will likely continue until after glaciers have fully disappeared.

Data availability. The rockfall inventory can be downloaded from the *mediaTUM* data repository under the following weblink: https://mediatum.ub.tum.de/1540134.

Author contributions. MKE, LS and JO initiated the underlying research project in 2010 and obtained the funding. MKE, IH and RD developed the idea and designed the study. IH and RD conducted the data acquisition and the data analysis. All authors contributed to the discussion and interpretation of the data. IH drafted the manuscript with significant contributions from MKR and AL.

Competing interests. The authors declare that they have no conflict of interest.

Acknowledgements. A. Schober kindly provided the photographs used for Fig. 2.

Financial support. This study was co-funded by the Austrian Academy of Sciences (ÖAW) (Project 'GlacierRocks'), the
Arbeitsgemeinschaft Alpenländer (ARGE ALP) (Project 'CirqueMonHT') and the Austrian Research Promotion Agency
(FFG) (Project 'MOREXPERT'). We furthermore thank the Gletscherbahnen Kaprun AG (Project 'Open-Air-Lab
Kitzsteinhorn') for financial and logistical support.

References

Abellán, A., Calvet, J., Vilaplana, J. M., and Blanchard, J.: Detection and spatial prediction of rockfalls by means of terrestrial
laser scanner monitoring, GEOMORPHOLOGY, 119(3-4), 162-171, 2010.

Abellán, A., Vilaplana, J. M., Calvet, J., García-Sellés, D., and Asensio, E.: Rockfall monitoring by Terrestrial Laser Scanning
– case study of the basaltic rock face at Castellfollit de la Roca (Catalonia, Spain), NAT HAZARD EARTH SYS, 11(3), 829-
841, 2011.

Allen, S. K., Cox, S. C., and Owens, I. F.: Rock avalanches and other landslides in the central Southern Alps of New Zealand:
a regional study considering possible climate change impacts, LANDSLIDES, 8(1), 33-48, 2010.

Andrews, J. T. and LeMasurier, W. E.: Rates of Quaternary Glacial Erosion and Corrie Formation, Marie Byrd Land,
Antarctica. GEOLOGY, 1(2), 75-80, 1973.

Arenson, L. U., Philips, M., and Springman, S. M.: Geotechnical considerations and technical solutions for infrastructure in
mountain permafrost, in: New Permafrost and Glacier Research, edited by: Krugger, M. I. and Stern, H. P., Nova Science
Publishers, New York, USA, 3-50, 2009.

Ballantyne, C. K. and Benn, D. I.: Paraglacial Slope Adjustment and Resedimentation Following Recent Glacier Retreat,
Fabergstolsdalen, Norway, ARCTIC ALPINE RES, 26(3), 255-269, 1994.

Ballantyne, C. K.: Paraglacial geomorphology, QUATERNARY SCI REV, 21(18-19), 1935-20

Ballantyne, C. K.: Periglacial Geomorphology. John Wiley and Sons, Chichester, 2018.

Barlow, J., Lim, M., Rosser, N., Petley, D., Brain, M., Norman, E., and Geer, M.: Modeling cliff erosion using negative power
law scaling of rockfalls, GEOMORPHOLOGY, 139-140, 416-424, 2012.

Barr, I. D. and Spagnolo, M.: Glacial cirques as palaeoenvironmental indicators: their potential and limitations, EARTH-SCI
REV, 151, 48-78, 2015.

Barsch, D.: Eine Abschätzung von Schuttproduktion und Schutttransport im Bereich aktiver Blockgletscher der Schweizer
Alpen, Z GEOMORPHOL, 28, 148-160, 1977.

Benn, D. I. and Evans, D. J. A.: Glaciers & Glaciation, Routledge Taylor & Francis Group, London and New York, 2010.

Bennett, M. R. and Glasser, N. F.: Glacial Geology, Wiley-Blackwell, Chichester, UK, 2009.

Bennett, G. L., Molnar, P., Eisenbeiss, H. and McArdell, B. W.: Erosional power in the Swiss Alps: characterization of slope failure in the Illgraben, EARTH SURF PROC LAND, 37(15), 1627-1640, 2012.

430 Bieniawski, Z. T.: Classification of Rock Masses for Engineering: The RMR System and Future Trends, in: Comprehensive rock engineering, Principles, practice & projects, edited by: Hudson, J. A. and Brown E. T., First Edition, Pergamon Press, New York, USA, 553-573, 1993.

Bommer, C., Phillips, M., and Arenson, L. U.: Practical recommendations for planning, constructing and maintaining infrastructure in mountain permafrost, PERMAFROST PERIGLAC, 21(1), 97-104, 2010.

435 Brocklehurst, S. H. and Whipple, K. X.: Glacial erosion and relief production in the Eastern Sierra Nevada, California, GEOMORPHOLOGY, 42(1-2), 1-24, 2002.

Brook, M. S., Kirkbride, M. P., and Brock, B. W.: Cirque development in a steadily uplifting range: rates of erosion and long-term morphometric change in alpine cirques in the Ben Ohau Range, New Zealand, EARTH SURF PROC LAND, 31(9), 1167-1175, 2006.

440 Chen, Y. and Medioni, G.: Object modelling by registration of multiple range images, IMAGE VISION COMPUT, 10(3), 145-155, 1992.

Clauset, A., Shalizi, C. R., and Newman, M. E. J.: Power-Law Distributions in Empirical Data, SIAM REV, 51(4), 661-703, 2009.

Cornelius, H. and Clar, E.: Erläuterungen zur geologischen Karte des Glocknergebietes, Geologische Bundesanstalt, Vienna,
445 32 pp., 1935.

Cossart, E., Braucher, R., Fort, M., Bourlès, D. L., and Carcaillet, J.: Slope instability in relation to glacial debuttressing in alpine areas (Upper Durance catchment, southeastern France): Evidence from field data and 10Be cosmic ray exposure ages, GEOMORPHOLOGY, 95(1-2), 3-26, 2008.

Crest, Y., Delmas, M., Braucher, R., Gunnell, Y., and Calvet, M.: Cirques have growth spurts during deglacial and interglacial
450 periods: Evidence from 10Be and 26Al nuclide inventories in the central and eastern Pyrenees, GEOMORPHOLOGY, 278, 60-77, 2017.

de Haas, T., Conway, S. J., and Krautblatter, M.: Recent (Late Amazonian) enhanced backweathering rates on Mars: Paracratering evidence from gully alcoves, J GEOPHYS RES-PLANET, 120(12), 2169-2189, 2015.

Delmas, M., Calvet, M., and Gunnell, Y.: Variability of Quaternary glacial erosion rates – A global perspective with special
455 reference to the Eastern Pyrenees, QUATERNARY SCI REV, 28(5-6), 484-498, 2009.

Densmore, A. L., Anderson, R. S., McAdoo, B. G., and Ellis, M. A.: Hillslope Evolution by Bedrock Landslides, SCIENCE, 275(5298), 369-372, 1997.

Derron, M.-H. and Jaboyedoff, M.: Preface "LIDAR and DEM techniques for landslides monitoring and characterization", NAT HAZARD EARTH SYS, 10(9), 1877-1879, 2010.

460 Draebing, D. and Krautblatter, M.: The Efficacy of Frost Weathering Processes in Alpine Rockwalls, GEOPHYS RES LETT, 46(12), 6516-6524, 2019.

Dussauge-Peisser, C., Helmstetter, A., Grasso, J.-R., Hantz, D., Desvarreux, P., Jeannin, M., and Giraud, A.: Probabilistic approach to rock fall hazard assessment: potential of historical data analysis, NAT HAZARD EARTH SYS, 2, 15-26, 2002.

Dussauge, C., Grasso, J.-R., and Helmstetter, A.: Statistical analysis of rockfall volume distributions: Implications for rockfall dynamics, J GEOPHYS RES-SOL EA: Solid Earth, 108(B6), 2003.

Duca, S., Occhiena, C., Mattone, M., Sambuelli, L., and Scavia, C.: Feasibility of Ice Segregation Location by Acoustic Emission Detection: A Laboratory Test in Gneiss, PERMAFROST PERIGLAC, 25(3), 208-219, 2014.

Evans, I. S.: Process and form in the erosion of glaciated mountains, in: Process and Form in Geomorphology, edited by: Stoddart, D. R., Routledge, London, UK, 145–174, 1997.

Evans, I. S.: Allometric development of glacial cirque form: Geological, relief and regional effects on the cirques of Wales, GEOMORPHOLOGY, 80(3-4), 245-266, 2006.

Ewald, A., Hartmeyer, I., Keuschnig, M., Lang, A., and Otto, J.-C.: Fracture Dynamics In An Unstable, Deglaciating Headwall, Kitzsteinhorn, Austria, EGU General Assembly, Vienna, Austria, 7–12 April 2019, EGU2019-3055, 2019.

Federici, P. R. and Spagnolo, M.: Morphometric analysis on the size, shape and areal distribution of glacial cirques in the maritime alps (western french-italian alps), GEOGR ANN A, 86(3), 235-248, 2004.

Fischer, A., Olefs, M., and Abermann, J.: Glaciers, snow and ski tourism in Austria's changing climate, ANN GLACIOL, 52(58), 89-96, 2011.

Fischer, A., Patzelt, G., Achrainer, M., Groß, G., Lieb, G. K., Kellerer-Pirklbauer A., and Bendler G.: Gletscher im Wandel: 125 Jahre Gletschermessdienst des Alpenvereins, Springer Spektrum, Berlin, Heidelberg, Germany, 2018.

Fischer, L., Kääb, A., Huggel, C., and Noetzli, J.: Geology, glacier retreat and permafrost degradation as controlling factors of slope instabilities in a high-mountain rock wall: the Monte Rosa east face, NAT HAZARD EARTH SYS, 6(5), 761-772, 2006.

Fischer, L., Purves, R. S., Huggel, C., Noetzli, J., and Haeberli, W.: On the influence of topographic, geological and cryospheric factors on rock avalanches and rockfalls in high-mountain areas, NAT HAZARD EARTH SYS, 12(1), 241-254, 2012.

Francou, B. : L'eboulisation en Haute Montagne (Alpes, Andes). Contribution à l'etude du systeme corniche-eboulis en milieu periglaciaire, These d'Etat, Editec, Caen, France, 696 pp., 1988.

Gardner, J. S.: Evidence for Headwall Weathering Zones, Boundary Glacier, Canadian Rocky Mountains, J GLACIOL, 33(113), 60-67, 1987.

Gillespie, C. S.: Fitting Heavy Tailed Distributions: The poweRlaw Package, J STAT SOFTW, 64(2), 2015.

Grämiger, L., Moore, J. R., Gischig, V. S., and Loew, S.: Thermomechanical Stresses Drive Damage of Alpine Valley Rock Walls During Repeat Glacial Cycles, J GEOPHYS RES-EARTH, 123(10), 2620-2646, 2018.

Grout, M.: Amount and rate of Holocene cirque erosion, Northern Sangre de Cristo Mountains, Colorado, Geological Society of America Abstracts with Programs, 11, 273-274, 1979.

Guzzetti, F., Reichenbach, P., and Wieczorek, G. F.: Rockfall hazard and risk assessment in the Yosemite Valley, California, USA, NAT HAZARD EARTH SYS, 3(6), 491-503, 2003.

495   Hales, T. C. and Roering, J. J.: Climate-controlled variations in scree production, Southern Alps, New Zealand, GEOLOGY, 33(9), 701-704, 2005.

Hallet, B.: Glacial Abrasion and Sliding: their Dependence on the Debris Concentration in Basal Ice, ANN GLACIOL, 2, 23-28, 1981.

Hartmeyer, I., Keuschnig, M., and Schrott, L.: A scale-oriented approach for the long-term monitoring of ground thermal
500   conditions in permafrost-affected rock faces, Kitzsteinhorn, Hohe Tauern Range, Austria, AUSTRIAN J EARTH SCI, 105(2), 128-139, 2012.

Hartmeyer, I., Delleske, R., Keuschnig, M., Krautblatter, M., Lang, A., Schrott, L., and Otto, J.-C.: Current glacier recession causes significant rockfall increase: The immediate paraglacial response of deglaciating cirque walls, EARTH SURF DYNAM, submitted.

505   Heckmann, T., Bimböse, M., Krautblatter, M., Haas, F., Becht, M., and Morche, D.: From geotechnical analysis to quantification and modelling using LiDAR data: a study on rockfall in the Reintal catchment, Bavarian Alps, Germany, EARTH SURF PROC LAND, 37(1), 119-133, 2011.

Heim, A.: Bergsturz und Menschenleben, Beiblatt zur Vierteljahrschrift der Naturforschenden Gesellschaft Zürich 77, 218 pp., 1932.

510   Hicks, D. M., McSaveney, M. J., and Chinn, T. J. H.: Sedimentation in Proglacial Ivory Lake, Southern Alps, New Zealand, ARCTIC ALPINE RES, 22(1), 26-42, 1990.

Hoeck, V., Pestal, G., Brandmaier, P., Clar, E., Cornelius, H., Frank, W., Matl, H., Neumayr, P., Petrakakis, K., Stadlmann, T., and Steyrer, H.: Geologische Karte der Republik Österreich, Blatt 153 Großglockner, Geologische Bundesanstalt, Vienna, 1994.

515   Holm, K., Bovis, M., and Jakob, M.: The landslide response of alpine basins to post-Little Ice Age glacial thinning and retreat in southwestern British Columbia, GEOMORPHOLOGY, 57(3-4), pp.201-216, 2004.

Hooke, R. L.: Positive feedbacks associated with erosion of glacial cirques and overdeepenings, GEOL SOC AM BULL, 103(8), 1104-1108, 1991.

Hovius, N., Stark, C. P., and Allen, P. A.: Sediment flux from a mountain belt derived by landslide mapping, GEOLOGY,
520   25(3), 231-234, 1997.

Humlum, O.: The geomorphic significance of rock glaciers: estimates of rock glacier debris volumes and headwall recession rates in West Greenland, GEOMORPHOLOGY, 35(1-2), 41-67, 2000.

Hungr, O., Evans, S. G., and Hazzard, J.: Magnitude and frequency of rock falls and rock slides along the main transportation corridors of southwestern British Columbia, CAN GEOTECH J, 36(2), 224-238, 1999.

525   Iverson, N. R.: Potential effects of subglacial water-pressure fluctuations on quarrying, J GLACIOL, 37(125), 27-36, 1991.

Jaeckli, H.: Gegenwartsgeologie des bündnerischen Rheingebiets, ein Beitrag zur exogenen Dynamik alpiner Gebirgslandschaften, Beitraege zur Geologie der Schweiz, Geotechnische Serie 36, 136 pp., 1957.

Johnson, W. D.: The Profile of Maturity in Alpine Glacial Erosion, The Journal of Geology, 12(7), 569-578, 1904.

Kenner, R., Phillips, M., Danioth, C., Denier, C., Thee, P., and Zgraggen, A.: Investigation of rock and ice loss in a recently
530   deglaciated mountain rock wall using terrestrial laser scanning: Gemsstock, Swiss Alps, COLD REG SCI TECHNOL, 67(3),
157-164, 2011.

Keuschnig, M., Hartmeyer, I., Höfer-Öllinger, G., Schober, A., Krautblatter, M., and Schrott, L.: Permafrost-Related Mass
Movements: Implications from a Rock Slide at the Kitzsteinhorn, Austria, in: Engineering Geology for Society and Territory,
edited by: Lollino, G., Manconi, A., Clague, J. Shan, W., and Chiarle, M., Springer International Publishing, 1(48), 255-259,
535   2015.

Keuschnig, M., Krautblatter, M., Hartmeyer, I., Fuss, C., and Schrott, L.: Automated Electrical Resistivity Tomography
Testing for Early Warning in Unstable Permafrost Rock Walls Around Alpine Infrastructure, PERMAFROST PERIGLAC,
28(1), 158-171, 2016.

Korup, O.: Large landslides and their effect on sediment flux in South Westland, New Zealand, EARTH SURF PROC LAND,
540   30(3), 305-323, 2005.

Krautblatter, M. and Moser, M.: A nonlinear model coupling rockfall and rainfall intensity based on a four year measurement
in a high Alpine rock wall (Reintal, German Alps), NAT HAZARD EARTH SYS, 9(4), 1425-1432, 2009.

Krautblatter, M., Moser, M., Schrott, L., Wolf, J., and Morche, D.: Significance of rockfall magnitude and carbonate
dissolution for rock slope erosion and geomorphic work on Alpine limestone cliffs (Reintal, German Alps),
545   GEOMORPHOLOGY, 167-168, 21-34, 2012.

Krautblatter, M. and Moore, J. R.: Rock slope instability and erosion: toward improved process understanding, EARTH SURF
PROC LAND, 39(9), 1273-1278, 2014.

Lague, D., Brodu, N., and Leroux, J.: Accurate 3D comparison of complex topography with terrestrial laser scanner:
Application to the Rangitikei canyon (N-Z), ISPRS J PHOTOGRAMM, 82, 10-26, 2013.

550   Larsen, E. and Mangerud, J.: Erosion Rate of a Younger Dryas Cirque Glacier at Kråkenes, Western Norway, ANN GLACIOL,
2, 153-158, 1981.

Lato, M. J., Diederichs, M. S., Hutchinson, D. J., and Harrap, R.: Evaluating roadside rockmasses for rockfall hazards using
LiDAR data: optimizing data collection and processing protocols, NAT HAZARDS, 60(3), 831-864, 2011.

Leith, K., Moore, J. R., Amann, F., and Loew, S.: In situ stress control on microcrack generation and macroscopic extensional
555   fracture in exhuming bedrock, J GEOPHYS RES-SOL EA, 119(1), pp.594-615, 2014.

Lewis, W. V.: Glacial Movement by Rotational Slipping, GEOGR ANN A, 31, 146-158, 1949.

Lim, M., Petley, D. N., Rosser, N. J., Allison, R. J., Long, A. J., and Pybus, D.: Combined Digital Photogrammetry and Time-
of-Flight Laser Scanning for Monitoring Cliff Evolution, PHOTOGRAMM REC, 20(110), 109-129, 2005.

Lim, M., Rosser, N. J., Allison, R. J., and Petley, D. N.: Erosional processes in the hard rock coastal cliffs at Staithes, North
560   Yorkshire. GEOMORPHOLOGY, 114(1-2), 12-21, 2010.

Mair, D., Lechmann, A., Delunel, R., Yeşilyurt, S., Tikhomirov, D., Vockenhuber, C., Christl, M., Akçar, N., and Schlunegger, F.: The role of frost cracking in local denudation of steep Alpine headwalls over millennia (Mt. Eiger, Switzerland), Earth Surf. Dynam. Discuss., in review, 2019.

Malamud, B. D., Turcotte, D. L., Guzzetti, F., and Reichenbach, P.: Landslide inventories and their statistical properties, EARTH SURF PROC LAND, 29(6), 687-711, 2004.

Martonne, E.: Sur la formation des cirques, ANN GEOGR, 10(49), 10-16, 1901.

McColl, S. T.: Paraglacial rock-slope stability. GEOMORPHOLOGY, 153-154, 1-16, 2012.

Moore, J. R., Sanders, J. W., Dietrich, W. E., and Glaser, S. D.: Influence of rock mass strength on the erosion rate of alpine cliffs, EARTH SURF PROC LAND, 34(10), 1339-1352, 2009.

Nguyen, H. T., Fernandez-Steeger, T. M., Wiatr, T., Rodrigues, D., and Azzam, R.: Use of terrestrial laser scanning for engineering geological applications on volcanic rock slopes – an example from Madeira island (Portugal), NAT HAZARD EARTH SYS, 11(3), 807-817, 2011.

Noetzli, J., Hoelzle, M., and Haeberli, W.: Mountain permafrost and recent Alpine rock-fall events: a GIS-based approach to determine critical factors, in: Proceedings of the 8th International Conference on Permafrost, Zurich, Switzerland, 21-25 July, 2, 827-832, 2003.

Oppikofer, T., Jaboyedoff, M., and Keusen, H.-R.: Collapse at the eastern Eiger flank in the Swiss Alps, NAT GEOSCI, 1(8), 531-535, 2008.

Oppikofer, T., Jaboyedoff, M., Blikra, L., Derron, M.-H., and Metzger, R.: Characterization and monitoring of the Åknes rockslide using terrestrial laser scanning, NAT HAZARD EARTH SYS, 9(3), 1003-1019, 2009.

Oskin, M. and Burbank, D. W.: Alpine landscape evolution dominated by cirque retreat, GEOLOGY, 33(12), 933, 2005.

Plaesken, R., Keuschnig, M., and Krautblatter M.: Systematic derivation of anchoring forces in permafrost-affected bedrock, EGU General Assembly, Vienna, Austria, 23–28 April 2017, EGU2017-14476, 2017.

Purdie, H.: Glacier Retreat and Tourism: Insights from New Zealand, MT RES DEV, 33(4), 463-472, 2013.

Purdie, H., Gomez, C., and Espiner, S.: Glacier recession and the changing rockfall hazard: Implications for glacier tourism, NEW ZEAL GEOGR, 71(3), 189-202, 2015.

Rabatel, A., Deline, P., Jaillet, S., and Ravanel, L.: Rock falls in high-alpine rock walls quantified by terrestrial lidar measurements: A case study in the Mont Blanc area, GEOPHYS RES LETT, 35(10), 2008.

Rapp, A.: Recent Development of Mountain Slopes in Kärkevagge and Surroundings, Northern Scandinavia, GEOGR ANN A, 42(2/3), 65-200, 1960.

Ravanel, L., Allignol, F., Deline, P., Gruber, S., and Ravello, M.: Rock falls in the Mont Blanc Massif in 2007 and 2008, LANDSLIDES, 7(4), 493-501, 2010.

Ravanel, L. and Deline, P.: Climate influence on rockfalls in high-Alpine steep rockwalls: The north side of the Aiguilles de Chamonix (Mont Blanc massif) since the end of the 'Little Ice Age', HOLOCENE, 21(2), 357-365, 2010.

Ravanel, L., Deline, P., Lambiel, C., and Vincent, C.: Instability of a high alpine rock ridge: the lower arête des cosmiques,
mont blanc massif, France, GEOGR ANN A, 95(1), 51-66, 2013.

Richter, E.: Geomorphologische Untersuchungen in den Hochalpen, PETERMANN GEOGR MITT, 29, 1-103, 1900.

Romana, M.: New adjustment ratings for application of Bieniawski classification to slopes, Proceedings of the International
Symposium on the Role of Rock Mechanics in Excavations for Mining and Civil Works, International Society of Rock
Mechanics, Zacatecas, pp.49-53, 1985.

Rosser, N. J., Petley, D. N., Lim, M., Dunning, S. A., and Allison, R. J.: Terrestrial laser scanning for monitoring the process
of hard rock coastal cliff erosion, Q J ENG GEOL HYDROGE, 38(4), 363-375, 2005.

Rosser, N. J., Lim, M., Petley, D. N., Dunning, S. A., and Allison, R. J.: Patterns of precursory rockfall prior to slope failure,
J GEOPHYS RES-EARTH, 112(F4), 2007.

Sadler, P. M.: Sediment Accumulation Rates and the Completeness of Stratigraphic Sections, The Journal of Geology, 89(5),
569-584, 1981.

Sanders, J. W., Cuffey, K. M., Moore, J. R., MacGregor, K. R., and Kavanaugh, J. L.: Periglacial weathering and headwall
erosion in cirque glacier bergschrunds, GEOLOGY, 40(9), 779-782, 2012.

Sanders, J. W., Cuffey, K. M., MacGregor, K. R., and Collins, B. D.: The sediment budget of an alpine cirque, GEOL SOC
AM BULL, 125(1-2), 229-248, 2012.

Sass, O.: Rock Moisture Fluctuations During Freeze-thaw Cycles: Preliminary Results from Electrical Resistivity
Measurements, Polar Geography, 28(1), 13-31, 2004.

Sass, O.: Spatial patterns of rockfall intensity in the northern Alps, Z GEOMORPHOL, 138, 51-65, 2005.

Sass, O. and Oberlechner, M.: Is climate change causing increased rockfall frequency in Austria?, NAT HAZARD EARTH
SYS, 12(11), 3209-3216, 2012.

Scherler, D., Bookhagen, B., and Strecker, M. R.: Hillslope-glacier coupling: The interplay of topography and glacial dynamics
in High Asia, J GEOPHYS RES-EARTH, 116(F2), 2011.

Schlögel, R., Torgoev, I., De Marneffe, C., and Havenith, H.-B.: Evidence of a changing size-frequency distribution of
landslides in the Kyrgyz Tien Shan, Central Asia, EARTH SURF PROC LAND, 36(12), 1658-1669, 2011.

Schober, A., Bannwart, C., and Keuschnig, M.: Rockfall modelling in high alpine terrain - validation and limitations /
Steinschlagsimulation in hochalpinem Raum - Validierung und Limitationen, Geomechanics and Tunnelling, 5(4), 368-378,
2012.

Stark, C. P. and Hovius, N.: The characterization of landslide size distributions, GEOPHYS RES LETT, 28(6), 1091-1094,
2001.

Stock, G. M., Bawden, G. W., Green, J. K., Hanson, E., Downing, G., Collins, B. D., Bond, S., and Leslar, M.: High-resolution
three-dimensional imaging and analysis of rock falls in Yosemite Valley, California, GEOSPHERE, 7(2), 573-581, 2011.

Strøm, K. M.: Geomorphology of the Rondane area, NORSK GEOL TIDSSKR, 25, 360–378, 1945.

Strunden, J., Ehlers, T. A., Brehm, D., and Nettesheim, M.: Spatial and temporal variations in rockfall determined from TLS measurements in a deglaciated valley, Switzerland, J GEOPHYS RES-EARTH, 120(7), 1251-1273, 2015.

Supper, R., Ottowitz, D., Jochum, B., Römer, A., Pfeiler, S., Kauer, S., Keuschnig, M., and Ita, A.: Geoelectrical monitoring

630   of frozen ground and permafrost in alpine areas: field studies and considerations towards an improved measuring technology, NEAR SURF GEOPHYS, 12(1), 93-115, 2013.

Terweh, S.: Geomorphologische Kartierung am Kitzsteinhorn (Hohe Tauern, Österreich) – Eine raum-zeitliche Analyse geomorphologischer Prozesse im Gletscherumfeld des Schmiedingerkees, Bachelor Thesis, University of Bonn, Germany, 67 pp., 2012.

635   van Veen, M., Hutchinson, D. J., Kromer, R., Lato, M., and Edwards, T.: Effects of sampling interval on the frequency - magnitude relationship of rockfalls detected from terrestrial laser scanning using semi-automated methods, LANDSLIDES, 14(5), 1579-1592, 2017.

Waldrop, H. A.: Arapaho Glacier: a sixty-year record. University of Colorado Studies, Series in Geology 3, 37 pp., 1964.

Williams, J. G., Rosser, N. J., Hardy, R. J., Brain, M. J., and Afana, A. A.: Optimising 4-D surface change detection: an

640   approach for capturing rockfall magnitude–frequency, EARTH SURF DYNAM, 6(1), 101-119, 2018.